Chem. Res. Chinese Universities, 2019, 35(4), 549—555 doi: 10.1007/s40242-019-9015-7

Carboxylate-induced Various Structures of Ni(II) Complexes with Fluorescence Sensing and Bifunctional Electrochemical Properties

LU Xue, LIU Guocheng*, WANG Xiang, LIN Hongyan and WANG Xiuli*

Liaoning Province Silicon Materials Engineering Technology Research Centre, Department of Chemistry, Bohai University, Jinzhou 121013, P. R. China

Abstract We synthesized three new Ni(II) coordination polymers $[Ni(L)(HIP)(H_2O)_2]\cdot H_2O$(CP**1**), $[Ni(L)(NIP)]\cdot 2H_2O$(CP**2**) and $[Ni(L)(NDC)(H_2O)_2]$(CP**3**)[L=*N*,*N*′-bis(pyridine-3-yl)thiophene-2,5-dicarboxamide, H_2HIP=5-hydroxyisophthalic acid, H_2NIP=5-nitroisophthalic acid, H_2NDC=2,6-naphthalenedicarboxylic acid] by hydrothermal method, which were characterized by means of infrared spectra(IR), TG analyses, PXRD and single-crystal X-ray diffraction. The CP**1** is a 1D tubular structure based on $[Ni\text{-}HIP]_2$ loops and pairs of L ligands. CP**2** is a 2D 3,5-connected architecture, which consists of Ni-L linear chains and $(Ni\text{-}NIP)_2$ double chains. CP**3** is a 2D network, which features 4-connected topology. Solid-state luminescent behaviours of CP**1**—CP**3** were investigated. The CP**1** can detect Fe^{3+} ions through luminescence quenching. The electrochemical properties of CP**1** buk-modified carbon paste electrode(CP**1**-CPE) has also been investigated, which has bifunctional electrocatalytic activity for oxidation of ascorbic acid and reduction of NO_2^-.

Keywords Carboxylate-induced; Coordination polymer; Fluorescent recognition; Bifunctional electrocatalysis

1 Introduction

Due to the important role of metal ions in environmental and biological systems, metal ion sensors have attracted extensive interest[1]. Fe^{3+} usually plays an important role in many biochemical processes of human body[2—4]. An excess or a deficiency of iron can affect the immune and enzyme systems of human body severely, which may lead to pathological disorders, including iron deficiency anemia, mental decline, etc.[5,6]. So, it is necessary to develop a sensor to detect the Fe^{3+} ion in aqueous media.

Recently, coordination polymers(CPs) have attracted much attention due to their applications in luminescence, fluorescence sensing and electrochemistry, as well as their fascinating structural diversity and topology characteristics[7—13]. Some CPs have been employed as fluorescence sensors because of their diverse structures and special properties[14—18]. However, building new CPs with sensing performance is still a challenging task. The main strategy to obtain CPs is designing or selecting suitable organic ligands.

Bis-pyridyl-bis-amide is a type of excellent organic ligands, because they possess not only diverse coordination groups, but also two types of hydrogen bonding sites(the —NH moieties and the —C═O groups), which are important for molecular recognition and the construction of supramolecular array[19]. The dicarboxylates are important multidentate O-donor ligands, which show diverse coordination modes and play an important role in the construction of CPs[20]. The combination of these two kinds of ligands gives a good opportunity to tune the architectures and properties of target CPs. Using the rigid/flexible bis-pyridyl-bis-amide and polycarboxyliate mixed ligands, our group has obtained a series of transition metal CPs[21—23]. Nevertheless, as far as we know, the report on the construction of Ni(II) CPs with semi-rigid thiophene-containing bis-pyridyl-bis-amide and dicarboxylic acid mixed ligands is still very limited.

In this work, the *N*,*N*′-bis(pyridine-3-yl)thiophene-2,5-dicarboxamide(L) was used as the main ligand, and three different dicarboxylic acids, 5-hydroxyisophthalic acid(H_2HIP), 5-nitroisophthalic acid(H_2NIP), 2,6-naphthalenedicarboxylic acid(H_2NDC) were selected as the co-ligands to react with Ni(II) ions. As a result, three new Ni(II) CPs, $[Ni(L)(HIP)\cdot(H_2O)_2]\cdot H_2O$(CP**1**), $[Ni(L)(NIP)]\cdot 2H_2O$(CP**2**) and $[Ni(L)\cdot(NDC)(H_2O)_2]$(CP**3**) were favourably constructed through hydrothermal reaction. The effects of polycarboxylate secondary ligands on the final structures of the three compounds were discussed, which eventually led to the different structures of CP**1**—CP**3**. Furthermore, the fluorescent properties and electrochemical behavior of CP**1**—CP**3** were investigated.

2 Experimental

2.1 Materials and Measurements

The ligand L was synthesized according to the previous

*Corresponding authors. Email: wangxiuli@bhu.edu.cn; lgch1004@sina.com

Received January 14, 2019; accepted March 28, 2019.

Supported by the National Natural Science Foundation of China(Nos.21671025, 21471021, 21401010).

literatures[24,25]. All other reagents and solvents for syntheses were purchased from Aladdin Industrial Co.(Shanghai) and used without purification. Elemental analyses(C, H, N) were carried out on a Perkin-Elmer 240C element analyser. Infrared spectra were measured on a 640 FTIR spectrometer. Powder X-ray diffraction(PXRD) data were taken on a D/teX Ultra diffractometer equipped with Cu $K\alpha$(λ=0.15406 nm) radiation. Thermal analysis was performed on a Pyris Diamond TG/DTA thermal analyser. The solid-state fluorescence spectra were measured with a Hitachi F-4500 fluorescence spectrophotometer at room temperature. The micro-sized crystal particles were prepared with the MSK-SFM-12M micro vibration ball mill. The electrochemical measurements were performed on a CHI 760 Electrochemical station. A conventional three-electrode cell was used at room temperature. The title complex bulk-modified carbon paste electrode was used as the working electrode. An SCE and a platinum wire were used as reference and auxiliary electrodes, respectively.

2.2 Synthesis of CP1

A mixture of $NiCl_2·6H_2O$(0.048 g, 0.2 mmol), L(0.032 g, 0.1 mmol), H_2HIP(0.018 g, 0.1 mmol) and NaOH(0.072 g, 1.8 mmol) in 9.2 mL of deionized water was stirred for 30 min at room temperature, then transferred to a 25 mL Telfon-lined stainless steel and heated in an oven to 120 °C for 5 d. After gradually cooling the autoclave to room temperature, the green block-shaped crystals were obtained with good reproducibility. Yield is 35%(based on Ni). Elemental anal.(%) calcd. for $C_{24}H_{22}N_4NiO_{10}S$: C 46.70, H 3.59, N 9.08; found: C 46.75, H 3.62, N 9.12. IR(KBr), $\tilde{\nu}$/cm^{-1}: 3842m, 3576w, 2923w, 2345m, 1830s, 1668s, 1650w, 1625m, 1537w, 1444m, 1432w, 1376w, 1314m, 1270w, 1196m, 1140m, 1009s, 929s, 891m, 866s, 835m, 779w, 736m, 698w, 642m, 562m.

2.3 Synthesis of CP2

The synthetic process of CP**2** was similar to that of CP**1**, except that H_2NIP(0.021 g, 0.1 mmol) was used instead of H_2HIP. Green block crystals of CP**2** were collected with good reproducibility. Yield is 15%(based on Ni). Elemental anal.(%) calcd. for $C_{24}H_{19}N_5NiO_{10}S$: C 45.89, H 3.05, N 11.15; found: C 45.92, H 3.09, N 11.18. IR(KBr), $\tilde{\nu}$/cm^{-1}: 3842m, 3619m, 2985m, 2351s, 1966s, 1768s, 1687m, 1682w, 1531w, 1494m, 1394w, 1320m, 1146s, 1010s, 909s, 767s, 729w, 593s.

2.4 Synthesis of CP3

The synthetic process of CP**3** was also similar to that of CP**1**, except that H_2NDC(0.022 g, 0.1 mmol) was employed instead of H_2HIP. Green block crystals of CP**3** were obtained with good reproducibility. Yield is 25%(based on Ni). Elemental anal.(%) calcd. for $C_{28}H_{22}N_4NiO_8S$: C 53.11, H 3.50, N 8.85; found: C 53.18, H 3.47, N 8.78. IR(KBr), $\tilde{\nu}$/cm^{-1}: 3387m, 1799s, 1672w, 1627m, 1546w, 1442s, 1408w, 1269w, 1362m, 1211w, 1320m, 1131s, 925m, 909s, 798m, 706m, 567s.

2.5 X-Ray Crystallography

The crystal structures of CP**1**—CP**3** were collected on a Bruker SMART APEXII diffractometer. The crystal structures were solved by direct methods using the SHELXS program of the SHELXTL crystallographic software package and refined on F^2 by full-matrix least-squares methods[26,27]. All non-hydrogen atoms were refined with anisotropic thermal parameters. The hydrogen atoms of the ligands were generated theoretically and treated isotropically. Details of the crystal parameters, data collection and refinements for CP**1**—CP**3** are listed in Table 1. Selected bond lengths and angles are shown in

Table 1 Crystal data and structural refinement for complexes CP1—CP3

Complex	CP**1**	CP**2**	CP**3**
Empirical formula	$C_{24}H_{22}N_4NiO_{10}S$	$C_{24}H_{19}N_5NiO_{10}S$	$C_{28}H_{22}N_4NiO_8S$
Formula weight	617.22	628.20	633.27
Crystal system	Orthorhomic	Triclinic	Triclinic
Space group	*Pccn*	$P\bar{1}$	$P\bar{1}$
T/K	296(2)	296(2)	296(2)
a/nm	2.1293(5)	1.00225(4)	0.93125(10)
b/nm	2.4383(5)	1.06610(5)	1.21943(13)
c/nm	0.9786(5)	1.30853(5)	1.32432(15)
α/(°)	90.00	75.913(1)	69.342(3)
β/(°)	90.00	77.856(1)	69.855(2)
γ/(°)	90.00	66.967(1)	82.747(3)
V/nm^3	5.081(3)	1.23758(9)	1.3211(2)
Z	8	2	2
D_c/(g·cm^{-3})	1.614	1.686	1.592
μ/mm^{-1}	0.912	0.939	0.874
F(000)	2544.0	644	652
θ_{max}/(°)	6320	4847	4676
R_{int}	0.042	0.0105	0.0392
$R_1{}^a$ [$I>2\sigma(I)$]	0.0332	0.0261	0.0526
$wR_2{}^b$(all data)	0.0881	0.0679	0.1429
Goodness-of-fit on F^2	1.000	1.031	1.030
Largest diff. peak/hole/(e·nm^{-3})	875/–906	904/–745	1050/–376

a. $R_1=\Sigma(||F_o|-|F_c||)/\Sigma|F_o|$; *b*. $wR_2=[\Sigma w(|F_o|^2-|F_c|^2)^2/(\Sigma w|F_o|^2)^2]^{1/2}$.

Table S1(see the Electronic Supplementary Material of this paper). CCDC reference numbers are 1877961 for CP**1**, 1877962 for CP**2** and 1877963 for CP**3**(http://www.ccdc.cam.ac.uk).

3 Results and Discussion

3.1 Crystal Structure

*3.1.1 [Ni(L)(HIP)(H_2O)$_2$]·H_2O(CP**1**)*

CP**1** shows the *Pccn* space group. As shown in Fig.1(A), CP**1** consists of one Ni(II) cation, one L, one HIP anion, two coordinated water molecules, and a crystalline water. Each Ni(II) center shows a six-coordinated distorted octahedral coordination geometry, coordinated by two pyridyl N atoms from two L ligands with Ni—N bond lengths of 0.2094(2) and 0.2139(2) nm, and four O atoms from two HIP anions and two water molecules, respectively. The bond lengths of Ni—O are in the range of 0.20716(17)—0.20866(19) nm.

Two HIP anions connect two Ni(II) ions to form [Ni-HIP]$_2$ ring[Fig.1(B)]. The L ligand adopting a μ_2-bridging mode links the adjacent [Ni-HIP]$_2$ rings to yield a 1D tubular structure [Fig.1(C)].

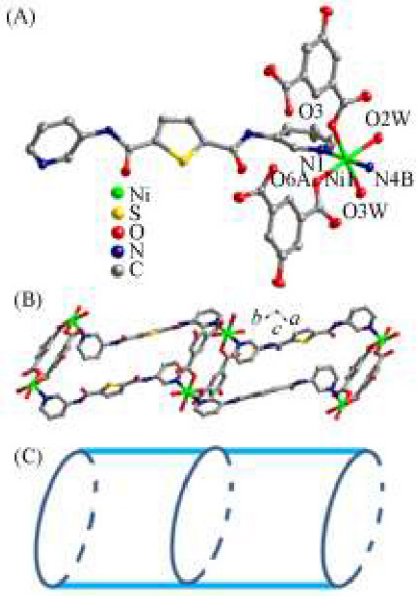

Fig.1 Coordination environment of Ni(II) ion(A), 1D double-stranded structure based on [Ni-HIP]$_2$ loops and pairs of L ligands(B) and schematic view of the 1D tubular structure(C) in CP1

*3.1.2 [Ni(L)(NIP)]·2H_2O(CP**2**)*

When H_2NIP was employed instead of H_2HIP under similar condition, a structurally different CP**2** was constructed, which belongs to $P\bar{1}$ space group. CP**2** is a 2D layer, which is composed of Ni-L linear chain and [Ni-NIP]$_2$ double chains. As indicated in Fig.2(A), CP**2** contains one Ni(II) ion, one L ligand, one NIP anion and two crystalline water molecules.

Each Ni(II) ion is six-coordinated by two pyridyl nitrogen atoms from two L ligands, the Ni—N bond distances are 0.21099(15) and 0.21125(15) nm, four oxygen atoms from three NIP anions with Ni—O bond distances of 0.19992(11) nm to 0.21687(11) nm.

In CP**2**, two carboxyl groups of each NIP anion exhibit the μ_1-η^1:η^1 and μ_2-η^1:η^1 modes to link the Ni(II) ions, building a 1D [Ni(NIP)]$_n$ chain[Fig.2(B)]. There exist two types of binuclear rings with different sizes in the 1D chain: a 16-membered loop {$Ni_2O_4C_{10}$} with approximate size of 0.862 nm×0.527 nm, another is an 8-membered loop {$Ni_2O_4C_2$} with the approximate size of 0.442 nm×0.429 nm. The L ligands with a bidentate bridging mode link the adjacent Ni(II) ions to yield a 1D [Ni(L)]$_n$ wave-like chain, which was further connected by the 1D [Ni(NIP)]$_n$ linear chains to form a 2D network[Fig.2(C)]. In case Ni(II) ions are designated as 5-connected nodes, NIP anions are regarded as three-connected nodes and L ligands are served as linear linkers, the overall network of CP**2** can be simplified as a (3,5)-connected {$4^2\cdot6^7\cdot8$}{$4^2\cdot6$} topology [Fig.2(D)].

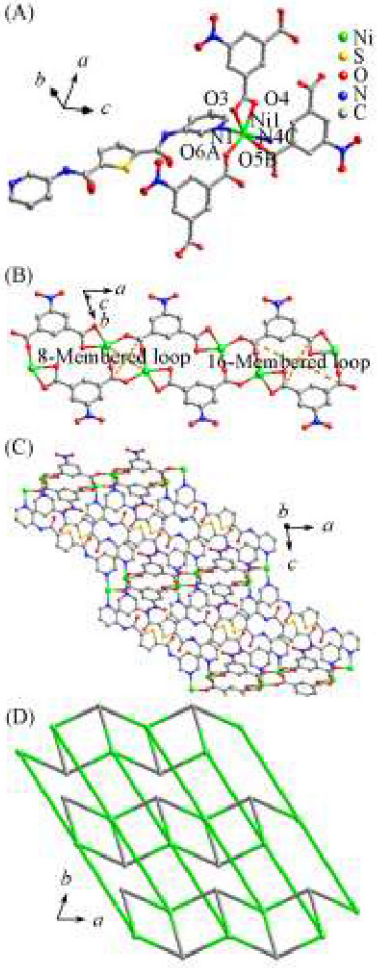

Fig.2 Coordination environment of Ni(II) ion(A), 1D [Ni(NIP)]$_n$ chain(B), 2D network extended by L and NIP double linkers(C) and schematic view of the 2D (3,5)-connected network(D) in CP2

*3.1.3 [Ni(L)(NDC)(H_2O)$_2$](CP**3**)*

CP**3** also belongs to the $P\bar{1}$ space group. As shown in Fig.3(A), the asymmetric unit of CP**3** consists of one Ni(II) cation, one L, one NDC anion and two coordinated water molecules. Each Ni^{II} center is six-coordinated by two nitrogen

atoms and four oxygen atoms, including two pyridyl nitrogen come from two L ligands[d(Ni—N1)=0.2142(3) nm], two carboxyl oxygen from two NDC anions with Ni—O bond lengths of 0.2043(3) and 0.2066(3) nm, and two oxygen atoms of two water molecules.

In CP**3**, the L ligands adopting a μ_2-mode connect the adjacent Ni(II) ions to generate a 1D $[Ni(L)]_n$ chain[Fig.3(B)]. The carboxyl groups from the NDC anions adopt bis(monodentate) modes bridging neighboring Ni(II) ions constructing a 1D $[Ni(NDC)]_n$ linear chain. The $[Ni(L)]_n$ chains and the linear $[Ni(NDC)]_n$ chains crossed with each other by sharing the Ni(II) ions, forming a 2D grid network[Fig.3(C)]. If the Ni(II) ion is regarded as a four-connector, both of L ligand and NDC anion are viewed as linear linkers, then the architecture of CP**3** is a 4-connected uninodal net with $\{4^4\cdot6^2\}$ topology[Fig.3(D)].

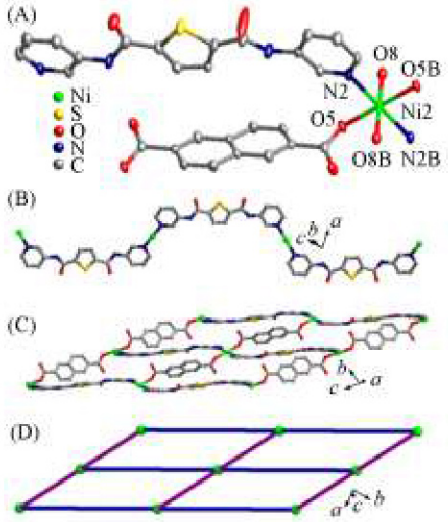

Fig.3 Coordination environment of Ni(II) ion(A), 1D $[Ni(L)]_n$ chain(B), 2D grid network(C) and schematic view of the 2D network(D) in CP3

3.2 Effects of the Polycarboxylic Anions on the Structures of the Title Complexes

Under the same synthesis conditions, by applying different aromatic polycarboxylic acid ligands, CP**1**—CP**3** with different structures were obtained. The structural differences between the CP**1**—CP**3** are shown in Scheme 1.

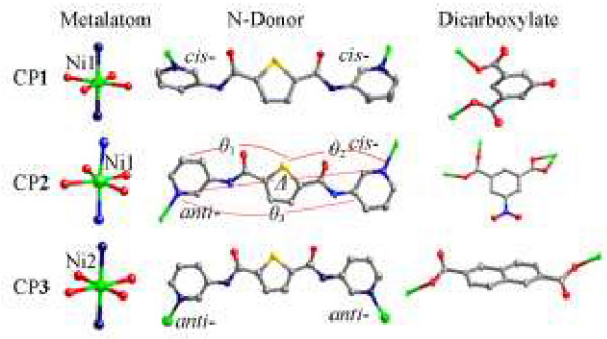

Scheme 1 Coordination modes of Ni(II) ions, L and polycarboxylates in CP1—CP3

In CP**1**, "V"-type carboxylate H_2HIP was used, in which HIP anion adopts a bis(monodentate) coordination mode, the L displays a bridging coordination mode, thus a 1D double-stranded structure was obtained, two pyridine nitrogen are in *cis*-mode relative to sulfur in the ligand. When NIP was selected as the co-ligand aiming at investigating the role of substituents in carboxylate on the structure of the target complex, a 3,5-connected 2D network was obtained, in which two pyridine nitrogen atoms adopt *anti*- and *cis*-modes. In CP**2**, the carboxyl groups of NIP anions adopt a monodentate and a chelating coordination mode. In order to study the effect of different aromatic polycarboxylates on the architectures of target complexes, a straight NDC anion was employed. As a result, a different 2D grid network of CP**3** was obtained. In CP**3**, two pyridine nitrogen atoms are both in *anti*-modes. The NDC anions adopt a bis(monodentate) bridging coordination mode.

In addition, we used θ to represent the twist degrees of pyridyl and thiophene groups of L and the Δ to represent the lengths between the N1 and N4 atoms in the pyridyl groups, as shown in Table S2(see the Electronic Supplementary Material of this paper) and Scheme 1. The differences in the θ angles and Δ lengths of title complexes can be attributed to different dicarboxylates. The results clearly indicate that various carboxylates show significant effects on the final structures of the title complexes(Scheme 2).

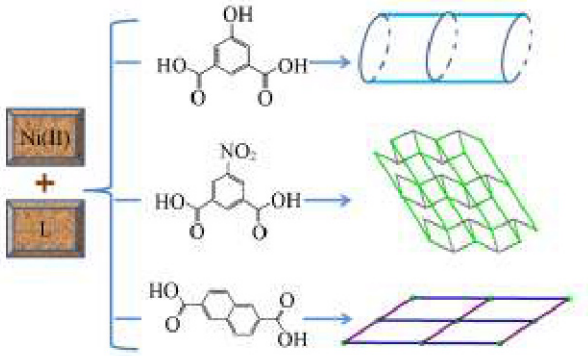

Scheme 2 Schematic view of the effect of polycarboxylates on the structures of CP1—CP3

3.3 IR, Powder X-Ray Diffraction and Thermal Stability Analysis

The IR spectra of CP**1**—CP**3** are measured in the frequency of 500—4000 cm^{-1}(Fig.S1, see the Electronic Supplementary Material of this paper). For L ligand, the characteristic peak of its carbonyl group is shown at 1649 cm^{-1} for CP**1**, 1636 cm^{-1} for CP**2**, 1672 cm^{-1} for CP**3**[28]. The peaks at 791 cm^{-1} for CP**1**, 742 cm^{-1} for CP**2**, 810 cm^{-1} for CP**3** can be attributed to the $\nu_{C—S}$ vibrations of thiophene ring of L ligand[29]. The distinct peaks at 1532 and 1432 cm^{-1} for CP**1**, 1537 and 1425 cm^{-1} for CP**2**, 1535 and 1340 cm^{-1} for CP**3** can put down to the asymmetric and symmetric vibrations of carboxyl groups[30]. For CP**1**—CP**3**, the peaks observed at 3301, 3407, and 3434 cm^{-1} suggest the presence of water molecules[30].

The experimental powder X-ray diffraction(PXRD) data were shown in Fig.S2(see the Electronic Supplementary Material of this paper), which is consistent with the simulated

patterns and verify the phase purity of CP**1**—CP**3**.

Thermal gravimetric(TG) analyses were carried out for CP**1**—CP**3** to examine their thermal stability(Fig.S3, see the Electronic Supplementary Material of this paper). The TG curves of CP**1**—CP**3** exhibit two different steps of mass loss processes. The mass loss of the first step occurred in 171—202 °C is 8.10% for CP**1**, 4.82% for CP**2** in the range of 104—136 °C and 5.1% for CP**3** in 210—250 °C, which can be attributed to the loss of the coordination or lattice water molecules(calcd. 8.75%, 5.73%, 5.68%). The second mass loss started at 341 °C for CP**1**, 400 °C for CP**2** and 333 °C for CP**3**, indicating the decomposition of organic components. The different decomposition temperatures and mass loss of the CP**1**—CP**3** may be due to the different structures and aromatic polycarboxylates in the title complexes[31].

3.4 Luminescent Property

In this work, the luminescence properties of CP**1**—CP**3** and L were measured in the solid state at ambient temperature. For CP**1** and CP**3**, the emission peaks are found at 461 and 448 nm(λ_{ex}=350 nm)(Fig.S4, see the Electronic Supplementary Material of this paper), which are red-shifted comparing with the free L ligand(λ_{em}=422 nm). Emission peak of CP**2** is found at 400 and blue-shifted comparing with the free L ligand (λ_{em}=422 nm)[19—21]. Ni(II) complexes do not contain d^{10} metal centers and their luminescence emissions are probably quenched by the Ni(II) ions[32]. The organic aromatic dicarboxylates usually exhibit weak $\pi^*\rightarrow n$ transitions and contribute little to the luminescence of CP**1**—CP**3**[33]. So the emissions of these three coordination polymers can be attributed to intra-ligand charge transitions of the L ligand. The different emission positions and intensities of CP**1**—CP**3** may be ascribed to the coordination environments of L, their different chemical species, as well as their diverse structures caused by the different polycarboxylates used in this work[34,35].

3.5 Fluorescent Sensing Property for Fe^{3+} Ion

Considering the good yield, water stability and the more potential recognition sites(hydroxyl of HIP and amide of L) in CP**1**, the fluorescent sensing property for metal cation of CP**1** was investigated. CP**1**(3 mg) was ground by vibrating ball mill for 30 min, and put into 0.01 mol/L MCl_x(M=Fe^{3+}, Fe^{2+}, Hg^{2+}, Mn^{2+}) or $M(NO_3)_2$(M=Cu^{2+}, Co^{2+}, Zn^{2+}, Ni^{2+}, Cd^{2+}, Cr^{3+}, Pb^{2+}) aqueous solution to form the M^{n+}@CP**1**. After being oscillated by ultrasound method for 30 min, the dispersion solution was generated for luminescent studies. The luminescent sensing behaviors of CP**1** toward various metal cations in aqueous solutions are described[Fig.4(A) and (B)].

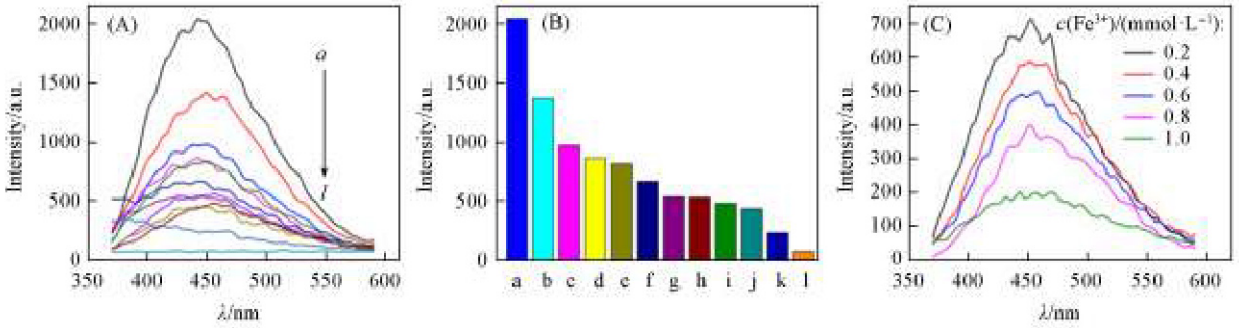

Fig.4 Luminescence spectra of M^{n+}@CP1(A) and the comparison of the luminescence intensity of M^{n+}@CP1 with different metal ions in aqueous solutions(B) and emission spectra of Fe^{3+}@ CP1 aqueous suspensions with the concentration of Fe^{3+} in the range of 0.2×10^{-3}—1.0×10^{-3} mol/L(C)

a and a. Pb^{2+}; *b* and b. Cr^{2+}; *c* and c. Mn^{2+}; *d* and d. CP**1**-H_2O; *e* and e. Cd^{2+}; *f* and f. Ni^{2+}; *g* and g. Hg^{2+}; *h* and h. Zn^{2+}; *i* and i. Fe^{2+}; *j* and j. Co^{2+}; *k* and k. Cu^{2+}; *l* and l. Fe^{3+}.

Obviously, Pb^{2+}, Cr^{3+} and Mn^{2+} ions exhibited slightly positive effects on the luminescent intensity of CP**1**, while in the presence of other metal ions(Cu^{2+}, Co^{2+}, Zn^{2+}, Ni^{2+}, Cd^{2+}, Fe^{2+}, Hg^{2+}, Fe^{3+}), the luminescence intensity of CP**1** is decreased. Although the degree of decrease varies, it is obvious that Fe^{3+} ions have a significant quenching effect on the luminescence of CP**1**, which implies the possible application of CP**1** for recognizing and sensing Fe^{3+} ion. In order to explore the sensitivity of CP**1** towards Fe^{3+}, the corresponding changes of the fluorescence emission spectra of CP**1** with the change of Fe^{3+} concentration from 0.2 mmol/L to 1.0 mmol/L were recorded. As shown in Fig.4(C), the fluorescence intensity of an emulsion of CP**1** decreased with increasing Fe^{3+} concentration (2×10^{-4}— 1×10^{-3} mol/L). When the concentration of Fe^{3+} was increased to 1 mmol/L, the fluorescence intensity of CP**1** was quenched to 72.4%. The decrease degree of luminescence intensity of CP**1** was approximately proportional to the concentration of Fe^{3+}. The luminescence quenching may be due to the metal ions interacting with sulfur atoms from the L ligand in CP**1**[36,37]. Moreover, the PXRD patterns of Fe^{3+}@CP**1** after sensing Fe^{3+} were measured, which are approximately similar to those of CP**1** merely with some differences in reflection intensity and position, demonstrating that the basic frameworks remain unchanged after the sensing of Fe^{3+} ions(Fig.S5, see the Electronic Supplementary Material of this paper). The above subtle differences may be due to the different orientation of the crystals in the powder samples CP**1** and the Fe^{3+} interaction with the corresponding complexes.

3.6 Electrochemical and Bifunctional Electrocatalytic Behavior of CP1

Due to the ability to undergo reversible single electron redox process, nickel coordination polymers have attracted

interest of electrochemical research[38]. Thus CP**1** modified carbon paste electrode(CPE) was prepared as a working electrode(CP**1**-CPE) and its electrochemical properties were studied in 0.01 mol/L H_2SO_4+0.5 mol/L Na_2SO_4 aqueous solution as an example. It is well known that no redox peak can be observed on the bare CPE within the potential range of 700—−100 mV. While CP**1**-CPE showed a pair of reversible redox peaks in the range of 700— −100 mV(Fig.5). The mean peak potential $E_{1/2}=(E_{pa}+E_{pc})/2$ is 281 mV for CP**1**-CPE(scan rate: 100 mV/s), this is the redox couple of Ni(III)/ Ni(II)[39,40]. Effect of scanning rate on the electrochemical behavior of CP**1**-CPE was investigated when the scanning rate varied from 20 mV/s to 500 mV/s in the same potential range and solution. The peak potentials change gradually: the cathodic peak potentials moved to negative direction while the anodic peak potentials moved to positive direction with scan rate increasing. The plots of peak currents *versus* scan rates were depicted in the inset of Fig.5. It can be clearly seen that both the cathodic and anodic peak currents were proportional to the scan rates, indicating the surface-controlled redox process of CP**1**-CPE.

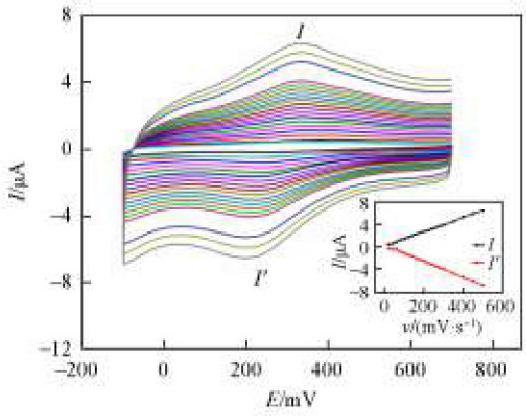

Fig.5 Cyclic voltammograms of CP1-CPE in 0.01 mol/L H_2SO_4+0.5 mol/L Na_2SO_4 aqueous solution at different scan rates(from inner to outer, 20 mV/s to 500 mV/s)

The inset shows the plots of the anodic and the cathodic peak currents *vs*. scan rate.

The electrocatalytic activitie of CP**1**-CPE in a 0.01 mol/L H_2SO_4+0.5 mol/L Na_2SO_4 aqueous solution toward the reduction of nitrite and oxidation of ascorbic acid(AA) were investigated in this work. In the potential range of –100—700 mV, a bare CPE shows no obvious response in a 0.01 mol/L H_2SO_4+0.5 mol/L Na_2SO_4 aqueous solution containing a 1.0 mmol/L AA or nitrite[38]. Fig.6 shows the cyclic voltammograms(CVs) of the CP**1**-CPE in the presence of AA. As can be clearly observed, the oxidation peak currents increase gradually and the corresponding reduction peak currents decrease with the addition of AA. The results suggest that CP**1**-CPE shows obvious electrocatalytic activity for the oxidation of AA[41]. As shown in Fig.7, the reduction peak currents of the CP**1**-CPE increase gradually when nitrite was added, while the oxidation peak currents decreased gradually. The results indicate that CP**1**-CPE could electrocatalyze the reduction of nitrite and can be used as the electrocatalyst. The cathodic peak is related to the irreversible reduction of NO_2^- to NO and then further reduction to N_2O in the acidic aqueous solution[42]. That is to say, the CP**1**-CPE could act as bifunctional electrocatalyst for the oxidation of AA and the reduction of nitrite.

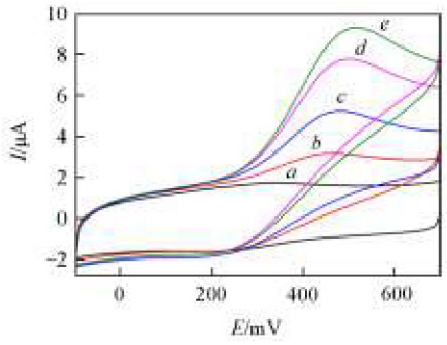

Fig.6 Cyclic voltammograms of CP1-CPE in 0.01 mol/L H_2SO_4+0.5 mol/L Na_2SO_4 aqueous solution containing 0(*a*), 2.0(*b*), 4.0(*c*), 6.0(*d*) and 8.0 mmol(*e*) of ascorbic acid

Scan rate: 100 mV/s.

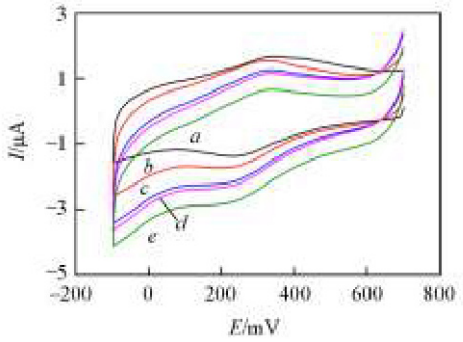

Fig.7 Cyclic voltammograms of CP1-CPE in 0.01 mol/L H_2SO_4+0.5 mol/L Na_2SO_4 aqueous solution containing 0(*a*), 2.0(*b*), 4.0(*c*), 6.0(*d*) and 8.0 mmol(*e*) of nitrite

Scan rate: 100 mV/s.

4 Conclusions

We synthesized three new Ni^{II} CPs from the semi-rigid bis-pyridyl-bis-amide L and different binary carboxylic acid under hydrothermal conditions. CP**1** is a 1D tubular chain, CP**2** is a 3,5-connected layer and CP**3** is a 4-connected network. The various architectures of CP**1**—CP**3** suggest that different organic polycarboxylic acids show great effect on the final various structures. The title complexes display luminescent properties. CP**1** shows fluorescent sensing behaviour for Fe^{3+} ions and its bulk-modified CPE shows good electrocatalytic activities toward the oxidation of AA and reduction of nitrite, demonstrating potential applications in electrocatalysis fields.

Electronic Supplementary Material

Supplementary material is available in the online version of this article at http://dx.doi.org/10.1007/s40242-019-9015-7.

References

[1] Liu X. F., Theil E. C., *Acc. Chem. Res*., **2005**, *38*(3), 167

[2] Liu J. Q., Li G. P., Liu W. C., Liu W. C., Li Q. L., Li B. H., Robert W. G., Hou L., Batten S. R., *ChemPlusChem*., **2016**, *81*(12), 1299

[3] Yan W., Zhang C., Chen S. G., Han L. J., Zheng H. G., *ACS Appl. Mater. Inter.*, **2017**, *9*(2), 1629

[4] Dang S., Ma E., Sun Z. M., Zhang H. J., *J. Mater. Chem.*, **2012**, *22*(33), 16920

[5] Hider R. C., Kong X. L., *Dalton Trans*., **2013**, *42*(9), 3220

[6] Carter K. P., Young A. M., Palmer A. E., *Chem. Rev.*, **2014**, *114*(8), 4564

[7] Wang X. L., Xiong Y., Sha X. T., Liu G. C., Lin H. Y., *Cryst. Growth Des*., **2017**, *17*(2), 483

[8] Kitagawa S., Kitaura R., Noro S., *Angew. Chem. Int. Ed.*, **2004**, *43*(18), 2334

[9] Liu Q., Yu L., Wang Y., Ji Y. Z., Horvat J., Cheng M. L., Jia X. Y., Wang G. X., *Inorg. Chem.*, **2013**, *52*(6), 2817

[10] Kreno L. E., Leong K., Farha O. K., Allendorf M., van Duyne R. P., Hupp J. T., *Chem. Rev*., **2012**, *112*(2), 1105

[11] Horcajada P., Serre C., Maurin G., Ramsahye N. A., Balas, F., Vallet-Regí M., Sebban M., Francis T., Gérard F., *J. Am. Chem. Soc.*, **2008**, *130*(21), 6774

[12] Chen B. L., Xiang S. C., Qian G. D. *Acc. Chem. Res*., **2010**, *43*(8), 1115

[13] Qiao Y., Ma Y. F., Jiang W., Wang X. Y., Guan W. S., Che G. B., Li W. K., Qin F., *CrystEngComm*., **2018**, *20*(48), 7782

[14] Chand S., Pal A., Pal S. C., Das M. C., *Eur. J. Inorg. Chem*., **2018**, *2018*(24), 2785

[15] Mahesh K., Karpagam S., *Sens. Actuators B: Chem*., **2017**, *251*, 9

[16] Rao P. C., Mandal S., *Inorg. Chem.*, **2018**, *57*(19), 11855

[17] Li Z., Li R., Li X. *Chem. J. Chinese Universities*, **2018**, *39*(11), 2363

[18] Zhang D. C., Xu Q. W., Li X., *Chem. J. Chinese Universities*, **2018**, *39*(12), 2611

[19] Lee C. H., Huang H. Y., Liu Y. H., Luo T. T., Lee G. H., Peng S. M., Jiang J. C., Chao I., Lu K. L., *Inorg. Chem*., **2013**, *52*(7), 3962

[20] Park M. K., Lim K. S., Park J. H., Song J. H., Kang D. W., Lee W. R., Hong C. S., *CrystEngComm*., **2016**, *18*(23), 4349

[21] Wang X. L., Wu X. M., Liu G. C., Lin H. Y., Wang X., *RSC Adv*., **2016**, *6*(88), 85030

[22] Wang X. L., Chen N. L., Liu G. C., Tian A. X., Sha X. T., Ma K. F., *Inorg. Chim. Acta*, **2015**, *432*, 128

[23] Wang X. L., Wu X. M., Liu G. C., Li Q. M., Lin H. Y., Wang X., *J. Solid State Chem.*, **2017**, *249*, 51

[24] Mu Y. J., Zhao Y. F., Xu H., Hou H. W., Fan Y. T., *J. Mol. Struct*., **2009**, *935*(1), 144

[25] Sarkar M., Biradha K., *Cryst. Growth Des*., **2006**, *6*(1), 202

[26] Sheldrick G. M., *Acta Crystallogr., Sect. A: Found. Crystallogr*., **2008**, *64*, 112

[27] Sheldrick G. M., *Acta Crystallogr., Sect. A: Found. Crystallogr*., **2015**, *71*, 3

[28] Dolensky B., Konvalinka R., Jakubek M., Kral V., *J. Mol. Struct*., **2013**, *124*, 1035

[29] Hipler F., Fischer R. A., Müller J., *J. Chem. Soc. Perkin Trans*., **2002**, *2*(2), 1620

[30] Bellamy L. J., *The Infrared Spectra of Complex Molecules*, Wiley, New York, **1958**

[31] Zhao Y., Wang L., Fan N. N., Han M. L., Yang G. P., Ma L. F., *Cryst. Growth Des.*, **2018**, *18*(11), 7114

[32] Heine J., Müller-Buschbaum K., *Chem. Soc. Rev*., **2013**, *42*(24), 9232

[33] Cui Y. J., Yue Y. F., Qian G. D., Chen B. L., *Chem. Rev*., **2012**, *112*(2), 1126

[34] Zou J. P., Peng Q., Wen Z. H., Zeng G. S., Xing Q. J., Guo G. C., *Cryst. Growth Des*., **2010**, *10*(6), 2613

[35] Gong Y., Wu T., Lin J. H., *CrystEngComm*., **2012**, *14*(10), 3727

[36] Jana A. K., Natarajan S., *ChemPlusChem.*, **2017**, *82*(8), 1153

[37] Staderini S., Tuci G., D'Angelantonio M., Manoli F., Manet I., Giambastiani G., Rossin A., *Chemistry Select*., **2016**, *6*(1), 1123

[38] Wang X. L., Ying X., Liu G. C., Lin H. Y., Wang X., *Dalton Trans.*, **2018**, *47*(29), 9903

[39] Singh A. K., Mukherjee R., *Dalton Trans*., **2005**, (17), 2886

[40] Pandey S., Das P. P., Singh A. K., Mukherjee R., *Dalton Tran*s., **2011**, *40*(40), 10758

[41] Zhang L., Dong S., *J. Electroanal. Chem.*, **2004**, *568*, 189

[42] Lin H. Y., Wang X. L., Hu H. L., Chen B. K., Liu G. C., *Solid State Sciences*, **2009**, *11*(3), 643